LAWRENCE
LIVERMORE
NATIONAL
LABORATORY

UCRL-JRNL-207911

Sulfur-induced corrosion of Au(111) studied by real-time STM

M.M. Biener, J. Biener, C.M. Friend

November 11, 2004

Topics in Catalysis

November 02, 2004

To be submitted to JACS

Sulfur-induced corrosion of Au(111) studied by real-time STM

Monika M. Biener[1,2], Juergen Biener[3,4] and Cynthia M. Friend[1,2, †]
[1]Department of Chemistry and
[2]Division of Engineering and Applied Sciences and
[3]Center for Imaging and Mesoscale Structures
Harvard University
12 Oxford Street, Cambridge, Massachusetts 02138 USA
[4]Nanoscale Synthesis and Characterization Laboratory
Lawrence Livermore National Laboratory
7000 East Ave, Livermore, CA 94550 USA

[†]Author to whom correspondence should be sent

Abstract

The interaction of sulfur with gold surfaces has attracted considerable interest due to numerous technological applications such as the formation of self-assembled monolayers (SAMs), use as a corrosion inhibitor, and as a chemical sensor.[1-3] In this work, the interaction of sulfur with Au(111) at two different temperatures (300 K and 420 K) was studied by real-time scanning tunnelling microscopy (STM), low energy electron diffraction (LEED) and Auger electron spectroscopy (AES). In the low coverage regime (< 0.1 monolayer), S modifies the surface stress leading to a lateral expansion of the Au surface layer. An ordered ($\sqrt{3}$x$\sqrt{3}$)R30° sulfur adlayer develops as the coverage reaches ~0.3 ML. With further increasing S coverage the Au(111) surface undergoes a dynamic rearrangement while forming a two-dimensional AuS phase: gold surface atoms are removed from regular terrace sites and incorporated into the growing gold sulfide phase resulting in the appearance of pits and irregularly shaped AuS islands. Gold sulfide prepared at room temperature exhibits short-range order; an incommensurate, long-range ordered AuS phase develops upon annealing at 450 – 525 K. Higher temperatures lead to decomposition of the AuS corrosion film. Formation of an ordered AuS phase via rapid step retraction rather than etch pit formation is observed during S-interaction with Au(111) surfaces *at* 420 K. Our results shed new light on the S-Au(111) interaction.

Introduction

Au is an important material in microelectronics due to its high electrical conductivity in combination with corrosion resistance. The noble character of Au does not imply a general inability to form stable bonds with non-metals but is rather a consequence of high reaction barriers towards dissociation reactions.[4] However, under certain circumstances Au surfaces can exhibit a high catalytic reactivity, and indeed Au-based catalysts are being developed for industrial oxidation processes.[5, 6] The Au-S interaction is probably the most intensively studied interaction of Au surfaces with a non-metal as it is important in numerous technological applications: Au ore formation,[7] thiol-based self-assembled monolayers (SAMs),[3, 8, 9] and corrosion inhibition, to name only a few. Furthermore, the increase of the electrical resistivity of thin gold films upon adsorption of certain sulphur-containing gases can be exploited to design sensors which allow the detection of minute traces of those species in gaseous mixtures.[2, 10] However, an atomic level picture of the underlying mechanism for the resistivity change has not been given yet, although numerous studies on the S/Au(111) interaction have been performed in recent years.

A very complex picture of the S/Au(111) interaction has emerged as demonstrated by the variety of surface structures formed when S is adsorbed under different experimental conditions.[1, 11-19] The majority of these structures were interpreted in terms of a "classic" surface model, where the positions of the Au atoms remain essentially unperturbed upon interaction with S. A common structure is the $(\sqrt{3}x\sqrt{3})R30°$ S adlayer with a coverage of 0.33 ML[1, 11, 13-15, 18] where sulfur atoms occupy threefold-hollow sites. This is also a commonly observed structure for alkanethiolate based SAMs on Au(111).[3] Ordered arrays of rectangular structures were observed at higher S coverages,[1, 11, 12, 14, 15] which were predominantly attributed to adsorbed S_8 species.

In the present study we used real-time STM in combination with low energy electron diffraction (LEED) and Auger electron spectroscopy (AES) to investigate both low and high S-coverage regimes. Real-time STM provides us with nano-scale, time resolved information and reveals the very dynamic character of the Au(111) surface upon interaction with sulfur, such as large-scale mass transport and incorporation of Au atoms in a growing AuS phase. In view of the typically observed inertness of Au surfaces the S-induced corrosion and mobilization of Au atoms is surprising and sheds new light on the nature of the Au-S interaction.

Experimental

All experiments were performed in an ultrahigh vacuum (UHV) system with a base pressure of $4x10^{-10}$ torr. The system is equipped with a home-made "beetle-type" STM and commercial instrumentation for AES and LEED. The sample was radiatively heated via a tungsten filament located behind the sample, and the temperature was monitored by a chromel/alumel thermocouple affixed to the sample holder. To account for the temperature gradient of the sample holder versus the crystal a calibration was performed using a thermocouple directly mounted to the crystal.

The Au sample was cleaned by cycles of Ar^+ sputtering (1000eV, ~5 μA) at 300 K, followed by annealing to 700 K for 10 minutes and 600 K for 60 minutes. This procedure was repeated several times until no contaminants were detected using AES. Following this procedure, the characteristic Au(111)-(22x√3) "herringbone" reconstruction was observed by LEED and STM. The Au sample used for the experiments of the present study exhibits many surface defects (see fig. 1 and 4), most likely partial Shockley dislocations[20] introduced by the gentle annealing procedures.

SO_2 (Matheson, anhydyrous grade) served as a source of sulfur, and was introduced using a leak valve such that a steady-state chamber pressure of $2x10^{-7}$ torr was maintained. Gas lines were evacuated before each dose. All exposures are given in uncorrected ion gauge readings using units of Langmuir ($1L=10^{-6}$ torr•s). Only a small fraction of the SO_2 molecules that impinge on the surface decomposes and deposits sulfur. The sulfur coverage was monitored by AES and calibrated relative to the (√3x√3)R30° LEED pattern which corresponds to a S coverage of 0.33 ML. The exposure of the surface to SO_2 was interrupted at various times and the surface examined using AES. The only species detected on the surface at all times was sulphur; oxygen, if any, was below the detection limit of AES. The oxygen released by SO_2 decomposition seems to be removed via an abstraction reaction with excess SO_2.[21] In order to rule out effects due to electron-induced reactions, the experiments were reproduced with the ion gauge turned off.

All STM images shown in this work were collected at room temperature or 420 K (if indicated) using $Pt_{0.8}$ $Ir_{0.2}$ tips. The tunneling bias was set in the range of +60 mV to +1.0 V. The STM scanner was calibrated against the unit cell of the Au(111) surface. Real-time STM images were collected during continuous SO_2 exposure. We observe the same S induced changes irrespective of whether the SO_2 exposure was prior to or during scanning.

Results and Discussion

The dynamic rearrangement of Au(111) surfaces with increasing S coverage at room temperature was captured by real-time STM imaging. The sequence of images displayed in figure 1 reveals a lifting of the herringbone reconstruction in the low S coverage regime followed by the formation of a 2D AuS phase at higher S coverages. The clean Au(111) surface exhibits a characteristic reconstruction pattern (fig. 1a, insert) that is caused by the incorporation of an additional 4% of Au atoms in the surface layer to reduce the tensile surface stress as described in detail elsewhere.[22, 23] This Au(111)-(√3x22) herringbone reconstruction is also signified by the presence of characteristic satellites spots in the LEED pattern shown in figure 2a.[24]

The surface stress of the clean Au(111) surface is modified upon sulfur adsorption. As a consequence, the herringbone reconstruction is lifted, even at S coverages as low as 0.1 ML. Au atoms, which are expelled during the surface relaxation,

agglomerate at the step edges thus causing a serrated (wavy) step-edge appearance (fig. 1b). Simultaneously the satellite spots in the LEED pattern associated with the herringbone structure disappear (fig 2b). The ejection of Au atoms revealed by STM indicates that S adsorption reverses the surface stress from tensile to compressive.

The origin of adsorbate-induced compressive surface stress can be understood in terms of a charge transfer from substrate surface bonds to the adsorbate atoms.[25] This in turn drives the ejection of Au atoms, which agglomerate at ascending step edges. Diffusion across descending steps at room temperature is hindered by the existence of a "Schwoebel" barrier. The amount of Au atoms as judged by the observed change in the step edge position during sulfur adsorption is consistent with the expected amount of ejected Au atoms (4%). The lifting of the Au(111) reconstruction by small amounts of strongly (specifically) adsorbed anions is also a common observation in electrochemical environments.[26]

An ordered (√3x√3)R30° sulfur adlayer develops as the S coverage approaches ~0.3 ML as inferred from the observation of a well-defined (√3x√3)R30° LEED pattern. As the LEED pattern develops, fractional-order spot-splitting is observed (figure 2c). Splitting of fractional-order spots can be explained by ordered arrays of antiphase domains[27], where the amount of splitting correlates with the domain size. The amount of splitting in our case corresponds to a (5x5) superlattice of the (√3x√3)R30° structure. The fractional-order spot-splitting disappears as the S coverage approaches 0.33 ML (fig. 2d).

The (√3x√3)R30° S adlayer observed by LEED is not observed using STM. Instead, atomically-resolved images of the Au surface were repeatedly obtained (figure 2c inset). These data indicate that the sulfur in the (√3x√3)R30° adlayer is too mobile to be imaged under the tunneling conditions used in the present work (see experimental). This is consistent with the streaky appearance of the STM images obtained in this coverage regime. A similar result was reported for K and Na (√3x√3)R30° adlayer phases on Au(111).[28, 29] However, the Au(111)-(√3x√3)R30°-S phase has been imaged by STM in an electrochemical environment.[1, 11, 14, 15]

Upon further increasing sulfur coverage we observe a dynamic surface restructuring caused by formation of a 2D AuS phase (figure 1d-f): small irregularly shaped islands start to nucleate, preferentially at defects, and monoatomic etch pits develop. Both pits and islands appear on terraces, and their density increases with increasing S-coverage (Fig. 1e). These observations indicate that there is massive mass transport: Au atoms are removed from regular terrace sites, thereby creating pits, and incorporated into the growing AuS phase. Finally the surface is completely covered with a 2D gold sulfide phase (Fig.1f) which exhibits a sponge-like morphology and passivates the Au surface against further corrosion. The S saturation coverage is 0.6 ML. The (√3x√3)R30° LEED pattern disappears (figure 2e) upon the formation of the first clusters, and a diffuse LEED pattern indicating missing long-range order is obtained.

The appearance of etch pits suggests that S continues to weaken the Au-Au bonds with increasing S coverage, finally reaching a point where the energy necessary to

remove Au atoms from regular lattice sites is overcompensated by the energy released by the formation of mobile Au-S species. This demonstrates that the Au-S bond is strong enough to drive the corrosion of Au. Indeed, stable gold sulfide clusters $(Au_2S)_n$, n = 1, 2, have been identified by ab initio calculations.[30] It is interesting that a preferred etching of Au step-edge atoms is not observed (see below).

The mobilization of Au surface atoms by the interaction with sulfur or sulfur-containing molecules seems to be a general phenomenon: For example, the formation of 2D vacancy islands of monoatomic depth has also been observed during the preparation of alkanethiol-based SAMs on Au(111).[8, 9, 31, 32] The driving force for the formation of these structures was, however, not clear; it was speculated that the vacancies may be related to a thiol-induced surface restructuring that enhances the Au surface diffusion rate. Mobilization of Au atoms and vacancy formation has also been observed during the interaction of cysteine with Au(110) surfaces.[33]

Significant changes in the surface topography are observed upon annealing: the sponge-like AuS phase formed at room temperature is transformed into an ordered two-dimensional AuS phase which produces a very complex, but well-defined LEED pattern (figure 2e). Simultaneously, large vacancy islands of monoatomic depth develop by Ostwald ripening of the irregular etch pits created during formation of the AuS phase at room temperature. Figure 3 shows the changes in the surface morphology as a function of the annealing temperature. Ring-like structures with some short-range order are observed after annealing to 420 K, and long-range order develops during annealing to 450 K. The growing vacancy islands are of monoatomic depth and both terraces and vacancy islands are uniformly covered by the AuS phase, based on the fact that the STM images are the same in vacancies and on terraces. The development of long-range order is further emphasized by the observation of a well-defined, complex LEED pattern (figure 2e).

The well-ordered AuS overlayer obtained after annealing exhibits a 1:1 stoichiometry: AES indicates a sulfur coverage of 0.5 ML, i.e. the sulfur coverage decreases by ~20% during annealing, in excellent agreement with the results obtained by a radioactive ^{35}S tracer-technique;[16, 17] the number of Au atoms incorporated in the 2D AuS phase was estimated to be 0.5 ML by determining the surface area covered by vacancy islands.

High-resolution STM images of the ordered 2D AuS phase reveal a quasi-rectangular unit cell, with lattice parameters of (8.8 ± 0.4) x (8.2 ± 0.4) $Å^2$ and an angle of 82° ± 4° between the lattice vectors (Figure 3e).The complex LEED pattern (figure 2f) is consistent with the STM results and can be interpreted in terms of an incommensurate AuS phase with a quasi-rectangular unit cell and 6 rotational domains. The orientation of one unit cell axes is rotated by ~7 degrees relative to the [110] direction of the Au substrate. This is consistent with the arrangement of rotational domains to each other as observed by STM. Interestingly, an early study reported a similar LEED pattern from Au(111) surfaces treated with H_2S/H_2 gas mixtures at elevated temperatures.[16, 17]

The ordered AuS phase described above seems to be a favorable configuration as very similar sulfur-induced surface structures on Au(111) have been prepared by electrooxidation in aqueous solutions of Na_2S or H_2S at room temperature.[1, 11, 12, 14, 15] The interpretation of these rectangular surface features is controversial although a model of adsorbed S_8 molecules was preferred by the majority of authors. However, the S-induced mobilization of Au atoms revealed by the present study clearly rules out a simple sulfur adlayer model.

In contrast to the UHV experiments presented here the ordered AuS phase develops without annealing in an electrochemical environment thus suggesting an increased surface mobility under these conditions. An anion-enhanced surface mobility is a common phenomenon in electrochemistry, and is indeed the basis of the so-called electrochemical annealing.[26, 34] It has been suggested that the increased mobility of Au surface atoms is caused by the anion-induced weakening of Au-Au surface bonds. This effect is more pronounced the more positive the potential and/or the stronger the anion-Au interaction.[26] Since the Au-S interaction is very strong, as demonstrated by the observed etching, it is not surprising that the ordered AuS phase can be formed in an electrochemical environment even at room temperature. However, the mass transport involved in the S-Au(111) interaction has not been reported earlier, and the majority of S-induced surface structures were consequently interpreted in terms of a simple adlayer surface model, where the positions of the Au atoms remain essentially unperturbed upon interaction with S.

The dynamic rearrangement of the Au surface upon interaction with S was further investigated by real-time scanning *at* 420 K. Figure 4 shows a series of STM images collected from a Au(111) surface as a function of increasing S coverage at 420 K. Using a defect (see arrow in fig. 4a) as reference point allows us to track changes in the step edge morphology during interaction with S. In the low coverage regime, the S-induced surface modifications are very similar to those observed during the corresponding room temperature experiments: the herringbone reconstruction is lifted, and Au atoms are ejected and agglomerate at step edges. Diffusion along step edges is fast at 420 K, and thus the step edges remain relatively straight (fig 4b), in contrast to the serrated step edge morphology observed during room temperature experiments (fig 1b). However, in the high coverage regime (~0.3 ML to ~0.5 ML) we detect a sudden retraction of step edges (figures 4c-f) rather than the etch pit and island formation observed at RT. After the step-edge position becomes stable again, indicating equilibrium, a S coverage of 0.5 ML was measured by AES (at 420 K). Despite missing evidence for AuS formation *at* 420K (except Au mobilization evidenced by step-retraction), the long-range ordered AuS phase described above is observed via LEED and STM *after* cooling the sample to room temperature (data not shown).

The sudden retraction of steps upon reaching a sulfur coverage of ~0.3 ML at 420 K is in contrast to the development of etch pits and islands at 300 K. The appearance of etch pits at 300 K indicates that Au atoms are pulled out of regular terrace sites, driven by the formation of stable AuS complexes which then nucleate to form irregularly shaped AuS islands. In contrast, at 420 K Au atoms in the surface layer seem to be mobile enough to annihilate any arising vacancy structure on the time scale of the experiment (~

2 min per frame), which leads to the impression of retracting step-edges. An alternative explanation would be that Au atoms are indeed supplied from weaker bound step edges sites. In this case, the absence of preferred step-edge etching at room temperature would indicate step-edge passivation by adsorbed AuS species or, alternatively, the development of a sulphur depletion zone at the step edge (diffusion-limited reaction regime).

The fate of the Au atoms which were removed from regular surface sites, but not detected as AuS islands as in the case of the room temperature experiment also needs to be considered. Since the amount of missing Au atoms is certainly too high to be explained in terms of mobile Au adatoms, we conclude that mobile AuS complexes are formed at 420 K. Upon cooling to room temperature a liquid-solid phase transition seems to take place. Alternatively, a coverage dependent liquid-solid phase transition could take place *at* 420 K, but this would require that the phase transition happens between two scans as otherwise we would have observed intermediate stages of the transition. Anyway, the ordered AuS thus obtained is identical to the AuS phase formed by room temperature reaction and subsequent annealing.

A quantitative analysis of the STM images shown in figure 4 reveals that the steps retract by ~ 0.5 ML equivalents (integrated area over the displacement of the step edges during S exposure). This is in excellent agreement with the surface area covered by vacancy islands after AuS formation at room temperature (figure 3c), and further corroborates our statement that 0.5 ML Au atoms are incorporated in the AuS phase.

The AuS phase is stable up to a temperature of ~ 525 K. During formation of the ordered AuS phase in the temperature range from 450 K to 525 K, the S coverage decreases by approx. 20% from 0.6 ML to 0.5 ML. Higher annealing temperatures cause a rapid decrease of the sulphur coverage. Simultaneously the well-defined LEED pattern (figure 2e) becomes diffuse. Figure 5 shows the S coverage as determined by the S_{150}/Au_{239} AES peak ratio versus annealing temperature.The sample was annealed for 20 minutes at each temperature and subsequently AE spectra were collected at room temperature. The loss of sulfur is most likely caused by the decomposition of the AuS corrosion film, rather than desorption of AuS units. Indeed, it has been reported that Au_2S decomposes into Au and S at temperatures above 490 K.[35]

Our results provide an atomic level picture of the working principle of Au-based sensors[10] for S containing gas species: a 2D AuS corrosion film is formed via massive mass transport at room temperature and decomposes above 525 K thereby restoring the sensing capacity. The AuS forms a pure 2D phase as it passivates the surface against further corrosion. This suggests that sensors with an enhanced sensitivity can be developed on the basis of nanoporous gold as this material exhibits a very high surface to volume ratio.

Conclusion

The results presented provide new insight into the S-Au(111) interaction. Sulfur interacts strongly with the Au(111) surface which leads to stress relaxation in the low S-coverage regime and corrosion involving a dynamic surface restructuring in the high S coverage

regime. Specifically, S adsorption lifts the herringbone reconstruction of the Au(111) surface even at a S coverage as low as 0.1 ML. The lifting of the herringbone reconstruction can be explained by a S-induced *weakening* of Au-Au surface bonds, which causes a lateral expansion of the Au surface layer. This reverses the surface stress from tensile to compressive as revealed by the ejection of Au atoms. As the S coverage approaches ~0.3 ML, an ordered ($\sqrt{3}$x$\sqrt{3}$)R30° sulfur adlayer develops. The S-induced weakening of Au-Au surface bonds continues with further increasing S coverage, which finally leads to the corrosion of the Au surface: gold surface atoms are removed from regular terrace sites and incorporated into the growing two-dimensional AuS phase resulting in the appearance of etch pits and irregularly shaped AuS islands. The development of the 2D AuS phase passivates the Au surface against further corrosion. Long-range order develops upon annealing at 450 – 525 K, higher temperatures lead to decomposition of the AuS corrosion film. A smooth, long-range ordered AuS phase without vacancy island structures can be prepared by S-interaction with Au(111) surfaces *at* 420 K.

Acknowledgements:

We gratefully acknowledge the support of this work by Harvard University NSEC, funded by the National Science Foundation, grant no. PHY-01-17795.
J. B. acknowledges current support under the auspices of the U. S. Department of Energy by the University of California, Lawrence Livermore National Laboratory, under Contract No. W-7405-Eng-48.

Figure captions

Figure 1: Real-time STM images capturing the dynamics of the S-induced Au corrosion at room temperature. (a) clean Au(111) surface exhibiting the typical herringbone reconstruction pattern (insert, 90 x 50 nm^2) caused by a 4% compression of the surface layer. (b) Even a small sulfur coverage (≤ 0.1 ML) reverses the surface stress from tensile to compressive and thereby drives the ejection of Au atoms. As a consequence the herringbone reconstruction is lifted (see insert, 75 x 40 nm^2). The ejected Au atoms agglomerate at ascending step edges leading to a serrated step edge appearance. (c) The unreconstructed Au(111) surface is stable up to a S coverage of ~ 0.3 ML, where S forms an ordered ($\sqrt{3}$x$\sqrt{3}$)R30° adlayer, which is transparent for STM (see atomically resolved Au surface in inset (2.6 x 1.5 nm^2)), but evident by LEED (fig. 2d). Early stages of the S-induced Au corrosion: (d) monoatomic etch pits and small AuS clusters appear on terraces, and (e) their density increases with increasing S-coverage. (f) At a sulfur coverage of ~0.6 ML the Au surface is covered with a sponge-like gold sulfide phase which passivates the surface against further corrosion.

Figure 2: Monitoring the S-induced corrosion of Au(111) by LEED: (a) clean, reconstructed Au(111) surface exhibiting the satellites of the Au(1,1) spots associated with the herringbone reconstruction. (b) The satellites disappear even at a low sulfur coverage (≤ 0.1 ML). (c) A (√3x√3)R30° pattern with split fractional-order spots develops, and (d) transforms into a regular (√3x√3)R30° pattern at a S-coverage of 0.33 ML. (e) With further increasing S coverage the LEED pattern becomes diffuse (0.33 ML $< \theta_S \leq$ 0.6 ML). (f) The well-defined complex LEED pattern observed after annealing to 450 K indicates the formation of an incommensurate AuS phase with long-range order ($\theta_S \sim$ 0.5 ML). All LEED images were obtained at an electron beam energy of 68 eV.

Figure 3: The morphology of the sponge-like AuS phase formed at room temperature (fig 1f) changes upon annealing. STM images were collected at room temperature after 10 min of annealing at 380 K (a), 420 K (b,c), and 450 K (d,e), respectively. With increasing annealing temperature, the original irregular etch pits transform into increasingly larger vacancy islands of monoatomic depth (Oswald ripening). Independent of the annealing temperature, the vacancy islands cover ~50% of the surface area, indicating the incorporation of ~0.5 ML of Au atoms into the 2D AuS phase. (c) After annealing to 420 K, some locally ordered arrays of quasi-rectangular structures can be observed by high-resolution STM. (e) Long-range order develops during annealing at 450 K. The AuS phase uniformly covers both vacancy islands and terrace areas.

Figure 4: Dynamic restructuring of the surface landscape upon interaction with S *at* 420 K, monitored by real-time STM: A surface defect (marked by the straight line) is used as reference point to track changes in the step morphology with respect to the original step edge structure (dashed lines), and to correct for the thermal drift of the experiment (note the lateral translation of the dashed lines in the different frames). (a) Clean Au(111) surface. (b) Sulfur lifts the reconstruction of the Au surface: the additional Au atoms incorporated in the reconstruction (4%) are ejected and agglomerate at ascending steps as evidenced by the outward flow of the steps. (c,d,e) With increasing S-coverage (0.3 ML to 0.5 ML) the steps suddenly retract indicating the removal of Au atoms from the surface layer and formation of a "liquid" AuS phase which is not visible in STM under the conditions of our experiments.

Figure **5**: The amount of S incorporated in the 2D AuS phase (prepared at room temperature) versus annealing temperature, as determined by the S_{150}/Au_{239} AES peak ratio (calibrated against the (√3x√3)R30° S adlayer with a S coverage of 0.33 ML). The sample was annealed for 20 minutes at each temperature and AE spectra were subsequently recorded at room temperature. Development of the long-range ordered AuS phase in the temperature range from 450 K to 525 K is accompanied by a decrease of the S coverage of approx. 20%. Higher annealing temperatures lead to a rapid loss of sulfur, most likely caused by AuS decomposition.

References

(1) Vericat, C., Vela M. E., Andreasen G., Salvarezza R. C., Vazquez L. and Martin-Gago J. A., *Langmuir* **2001**, *17*, 4919-4924.
(2) Yoo, K. S., Sorensen I. W. and Glaunsinger W. S., *J. Vac. Sci. Technol. A* **1994**, *12*, 192-198.
(3) Ulman, A., *Chem. Rev.* **1996**, *96*, 1533-1554.
(4) Hammer, B. and Norskov J. K., *Nature* **1995**, *376*, 238.
(5) Valden, M., Lai X. and Goodman D. W., *Science* **1998**, *281*, 1647-1650.
(6) Haruta, M., *Catal. Today* **1997**, *36*, 153-166.
(7) Phillips, G. N. and Evans K. A., *Nature* **2004**, *429*, 860.
(8) Poirier, G. E., *Langmuir* **1997**, *13*, 2026.
(9) Poirier, G. E., *Chem. Rev.* **1997**, *97*, 1117.
(10) *U.S. Patent No. 4724008*, (Arizona Instrument Corporation, 1988)
(11) Vericat, C., Andersen J. N., Vela M. E. and Salvarezza R. C., *J. Phys. Chem. B* **2000**, *104*, 302-307.
(12) McCarley, R. L., Kim Y. T. and Bard J., *J. Phys. Chem.* **1992**, *97*, 211.
(13) Martin, H., Vericat C., Andreasen G., Creus A. H., Vela M. E. and Salvarezza R. C., *Langmuir* **2001**, *17*, 2334-2339.
(14) Vericat, C., Vela M. E., Andreasen G. A. and Salvarezza R. C., *Phys. Rev. Lett.* **2003**, *90*, 075506.
(15) Gao, X., Zhang Y. and Weaver M. J., *J. Phys. Chem.* **1992**, *96*, 4156.
(16) Kostelitz, M. and Oudar J., *Surf. Sci* **1971**, *27*, 176.
(17) Kostelitz, M., Domange J. L. and Oudar J., *Surf. Sci.* **1972**, *34*, 431-449.
(18) Rodriguez, J. A., Dvorak J., Jirsak T., Gang L., Hrbek J., Aray Y. and Gonzalez C., *J. Am. Chem. Soc.* **2002**, *125*, 276-285.
(19) Touzov, I. and Gorman C. B., *Langmuir* **1997**, *13*, 4850.
(20) de la Fuente, O. R., Zimmerman J. A., Gonzalez M. A., de la Figuera J., Hamilton J. C., Pai W. W. and Rojo J. M., *Phys. Rev. Lett.* **2002**, *8803*, 6101.
(21) Biener, M. M., Biener J. and Friend C. M., *in preparation*
(22) Woell, C., Chiang R. J., Wilson J. and Lippel P. H., *Phys. Rev. B* **1989**, *39*, 7988.
(23) Barth, J. V., Brune H., Ertl G. and Behm R. J., *Phys. Rev. B* **1990**, *42*, 9307.
(24) Murty, M. V. R., Curcic T., Judy A. and Cooper B. H., *Phys. Rev. B* **1999**, *60*, 16956.
(25) Ibach, H., *Surf. Sci. Rep.* **1997**, *29*, 193.
(26) Kolb, D. M., *Prog. Surf. Sci.* **1996**, *51*, 109.
(27) Van Hove, M. A., Weinberg W. H. and Chan C. M., *Low-Electron Energy Diffraction* (Springer-Verlag, 1986).
(28) Barth, J. V., Behm R. J. and Ertl G., *Surf. Sci. Lett.* **1993**, *302*, L319-L324.
(29) Barth, J. V., Schuster R., Behm R. J. and Ertl G., *Surf. Sci.* **1995**, *348*, 280.
(30) Bagaturyants, A. A., Safonov A. A., Stoll H. and Werner H. J., *J. Chem. Phys.* **1998**, *109*, 3096.
(31) Poirier, G. E. and Pylant E. D., *Science* **1996**, *272*, 1145.
(32) Chailapakul, O., Sun L., Xu C. and Crooks R. M., *J. Am. Chem. Soc.* **1993**, *115*, 12459.

(33) Kuehnle, A., Linderoth T. R., Hammer B. and Besenbacher F., *Nature* **2002**, *415*, 891.
(34) Kolb, D. M., *Surf. Sci.* **2001**, *500*, 722.
(35) Ishikawa, K., Isonaga T., Wakita S. and Suzuki Y., *Solid State Ionics* **1995**, *79*, 60.

Fig. 1

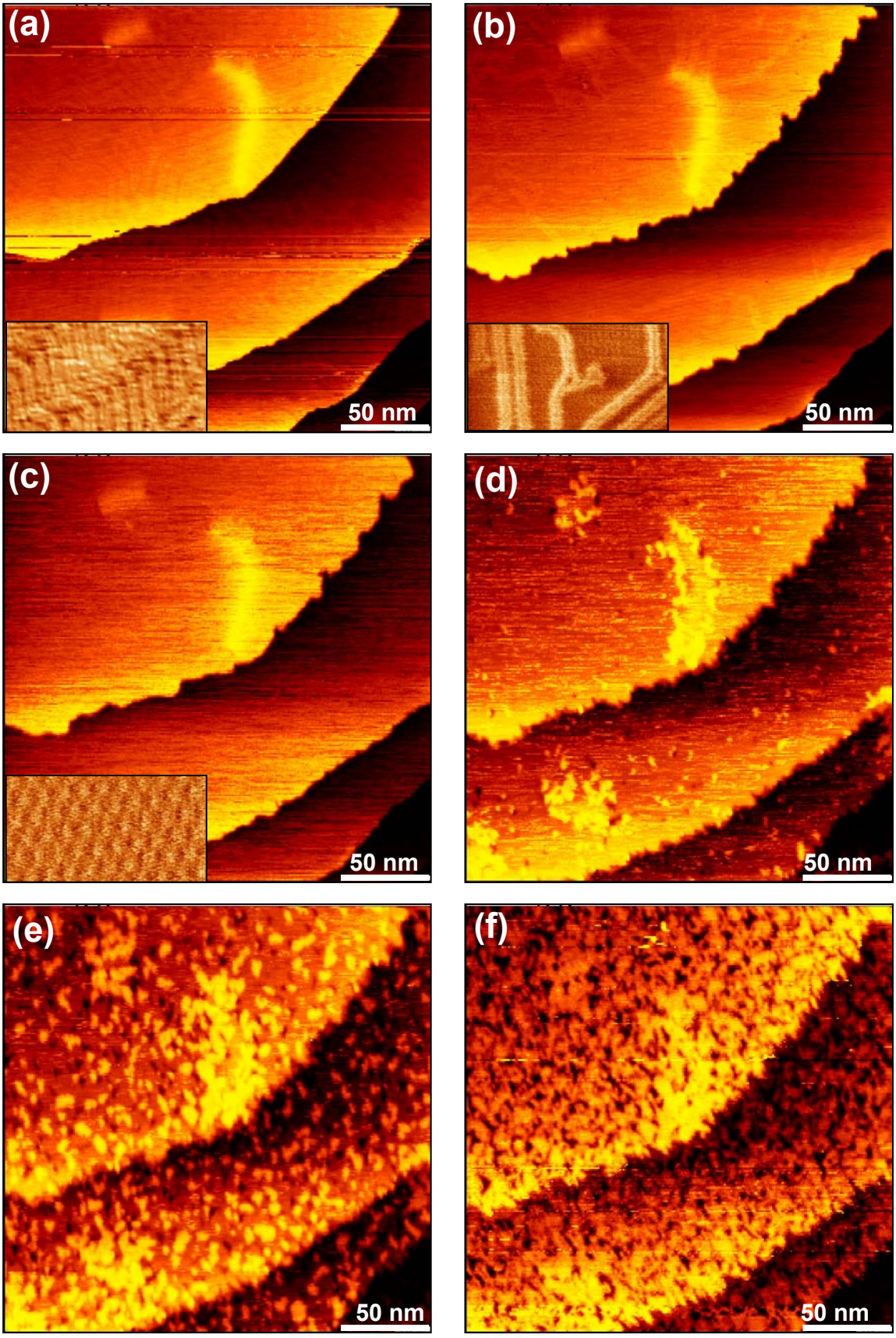

Fig. 2

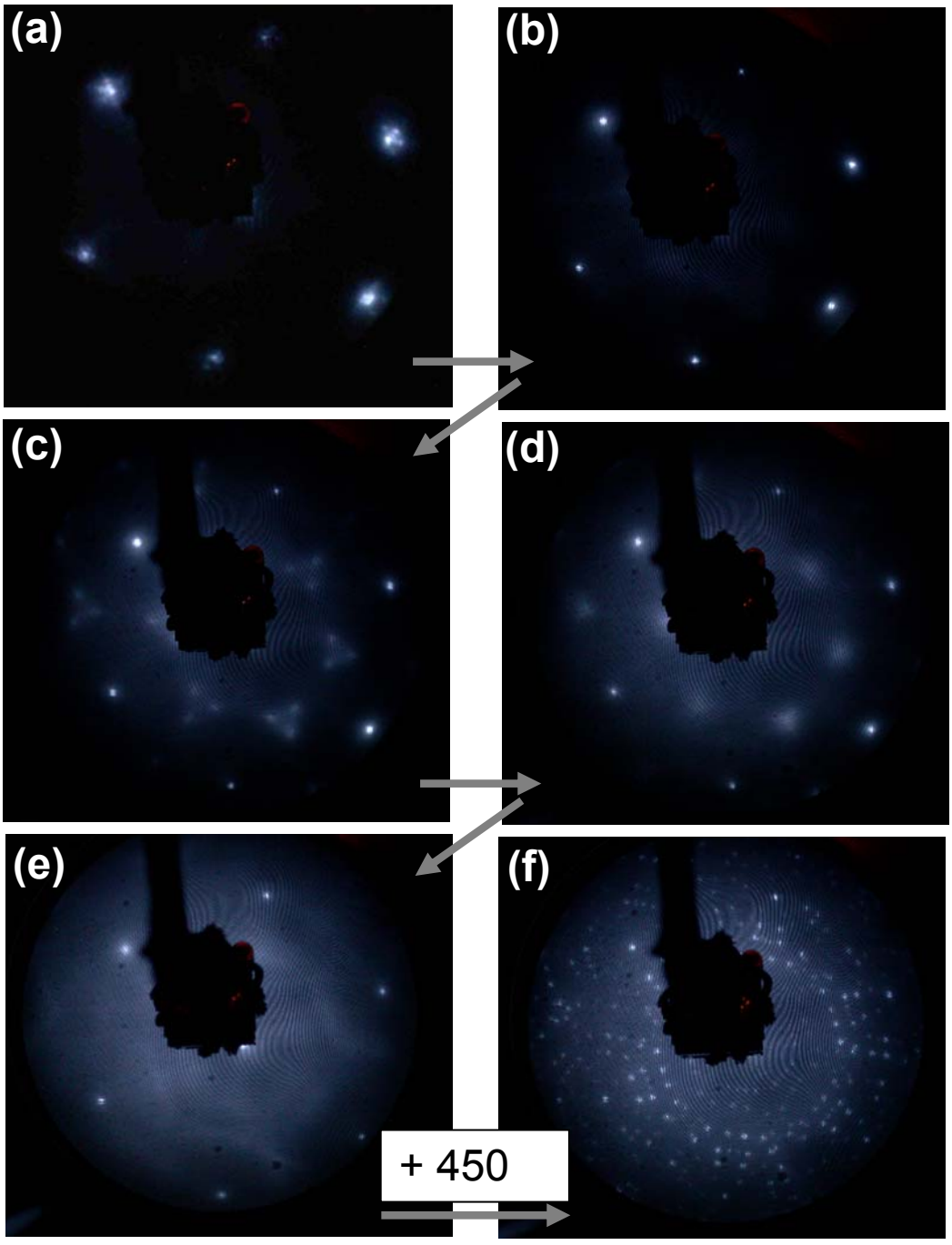

Fig. 3

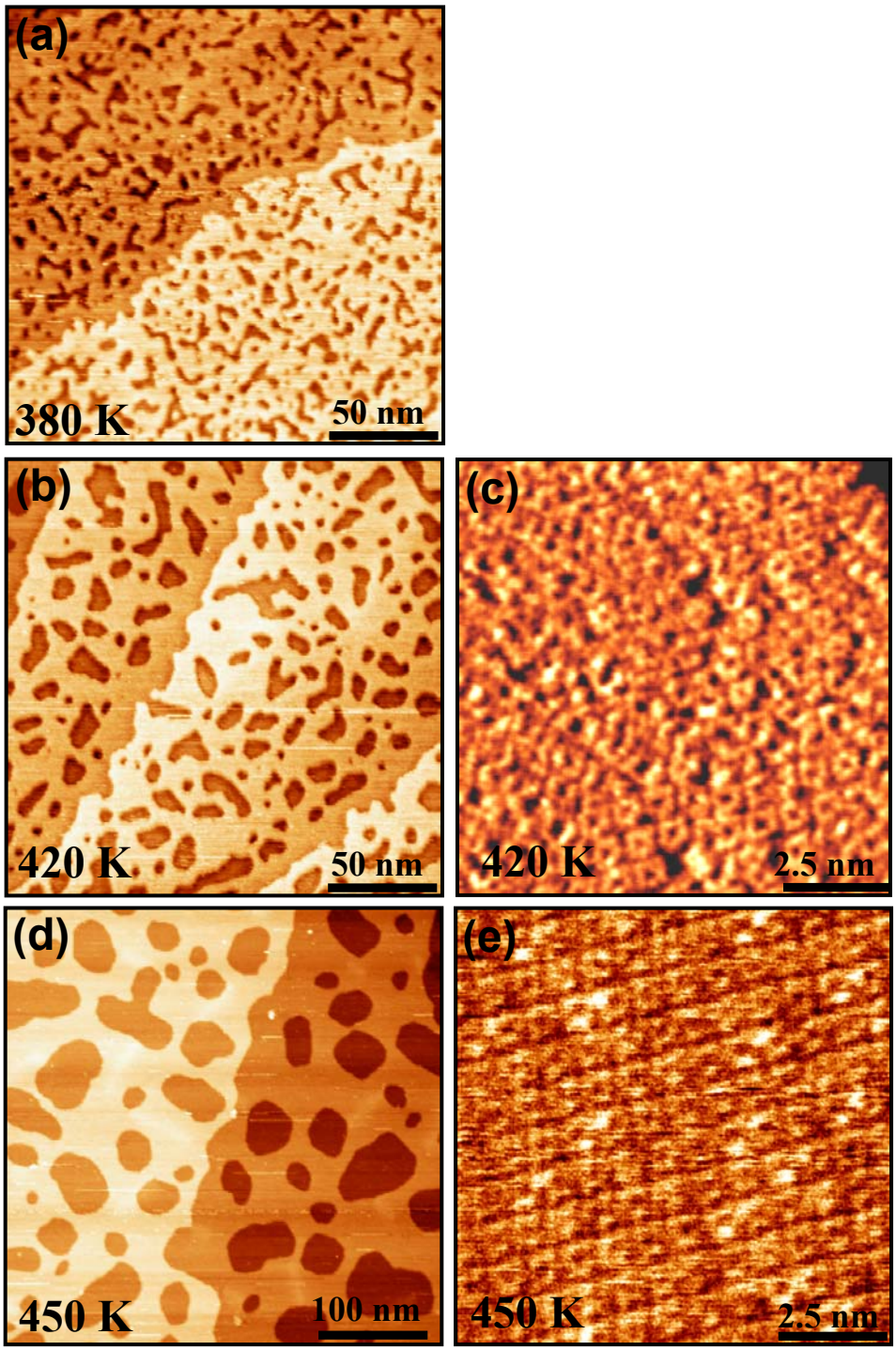

Fig. 4

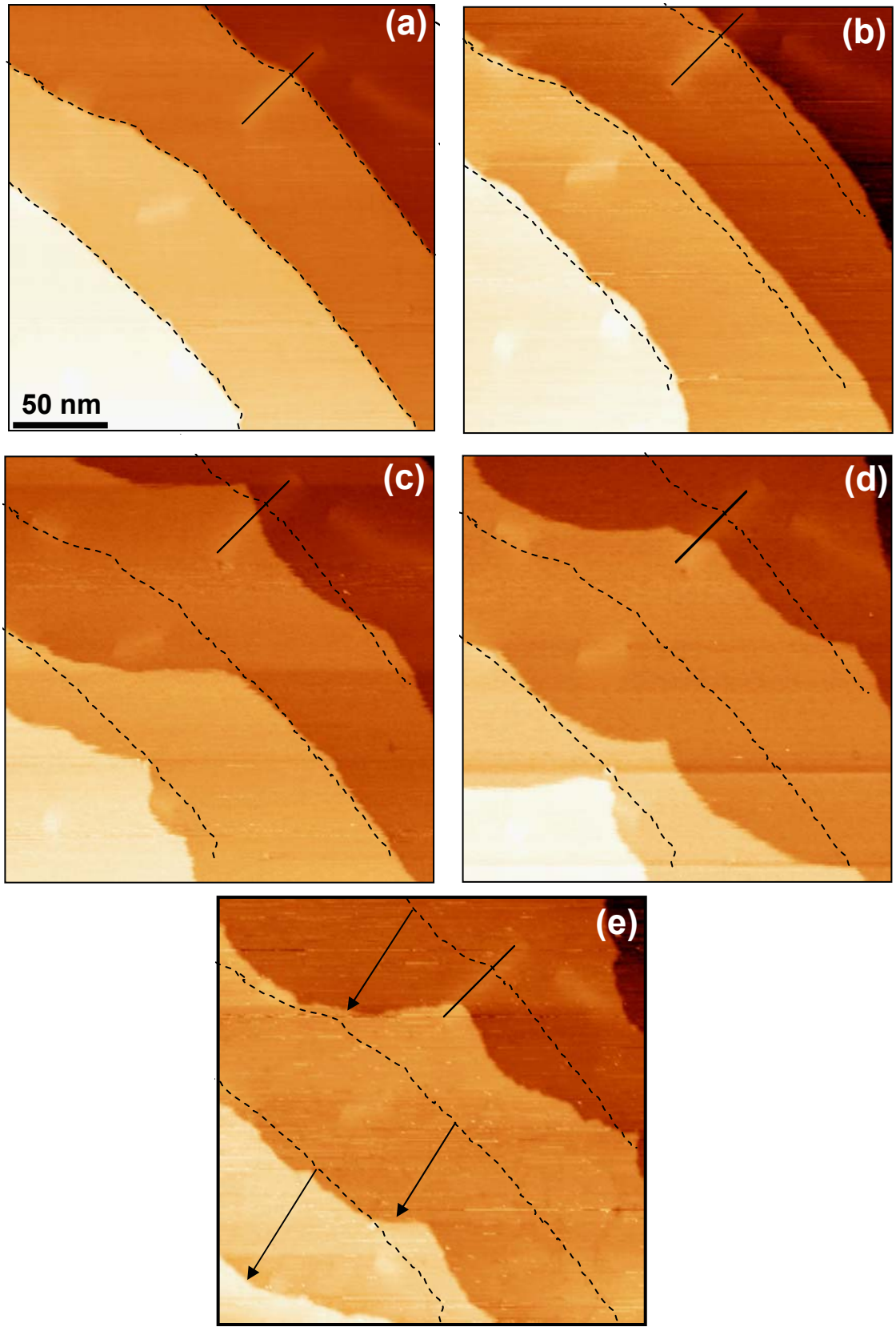

Fig. 5

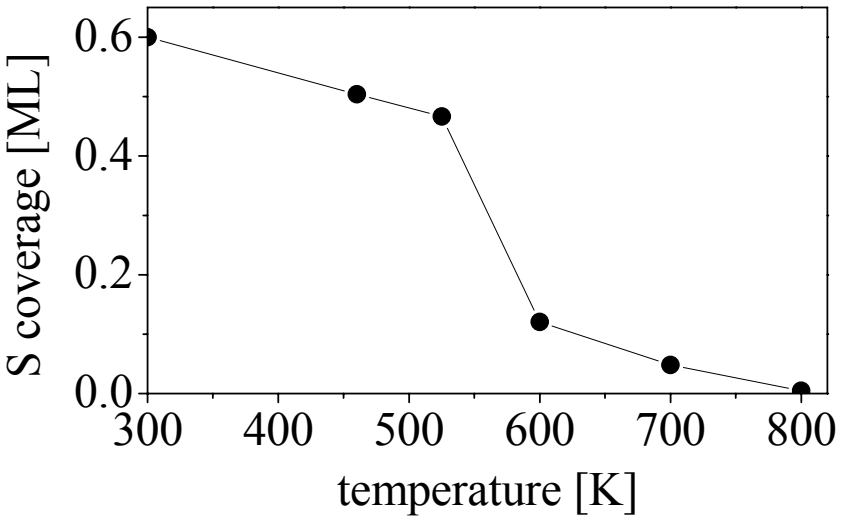

TOC image: